20

Softly Stable Walk Using Phased Compliance Control with Virtual Force for Multi-Legged Walking Robot

Qingjiu Huang
Tokyo Institute of Technology
Japan

1. Introduction

Recently, although the researches on the terrain adaptability of multi-legged walking robot have been widely performed (D. Wettergreen & C. Thorpe, 1996; T. Kubota, et al., 2000; Q. Huang, et al., 2000; Q. Huang & K. Nonami, 2000; Q. Huang & K. Nonami, 2003; K. Nonami & Q. Huang, 2003), it has not been put to be more widely practical use. This is because there are still some problems in the stable walking of multi-legged robot that need to be solved. For example, when the swing legs of robot moves, because the COG, supported weight, and moment of inertia of body change dynamically, the posture of robot body becomes unstable; furthermore, with the switch between the swing leg and the support leg, there occur the collisions and slippage between the foot and the ground. Because of the above uncertain disturbances, the tiny vibrations occur when the robot is walking. Until now, we proposed a robust control of posture and vibration based on a virtual suspension model for multi-legged walking robot to decrease the tiny vibrations when the robot walks (Q. Huang, et al., 2004; Q. Huang, et al., 2007). However, how to decrease the impact force between the foot and the terrain has not been solved yet. When the robot walks on irregular terrain or it bumps against the obstacle, due to the influence from the impact force between the foot and the ground, it is a possibility that the mechanical parts of robot are destroyed; moreover, the vibration in the robot body occurs and arouses the instability of posture. Therefore, it is necessary to decrease the impact force for the walking of the multi-legged robot.

Compliance control is one of the most effective control methods for the hand of manipulator to reduce impact force of contacting work (J. Huang, et al., 2002), because it can control relationship between the contact force and displacement of the hand. Recently, the compliance control was applied to biped walking robot (R. Quint, 1998). However, until now the compliance control is performed for decrease the vibration after impact force is generated, such as after the foot of the robot collides with the ground. It is impossible to reduce impact force perfectly as long as the compliance control is used after impact force is generated. So, counter measure which used the visual sensor to avoid object was proposed for manipulator in order to more effectively reduce the impact force (V. Mut, et al., 1998; X. Chen & H. Kano, 2005). And avoid action method that used virtual force to decelerate the

motion speed of hand was proposed (T. Tsuji, et al., 1997). However, these methods don't be applied to the legged walking robot, the problem on the impact force between the foot and the terrain when the foot lifting and landing aren't solved yet. Moreover, the robot motion can only move uniformity using the current compliance control method because it always keeps constant stiffness gain and viscous gain. Therefore, the current compliance control method can realize the target motion, but it is hard to decrease impact force for multi-legged walking robot.

In this chapter, in order to realize the softly stable walk of multi-legged robot, we introduce a phased compliance control with virtual compliance force to reduce impact force between the foot and unexpected ground and obstacle (Q. Huang, et al., 2008). Moreover, we show a design of hierarchical control system for multi-legged walking robot, which is combined the proposed phased compliance control with a posture and vibration control based on a virtual suspension model, to realize the stable walking on unknown rough terrain. Finally, the effectiveness of the above introduced method is discussed using the walking experimental results of the developed six-legged walking robot.

2. A Six-Legged Walking Robot

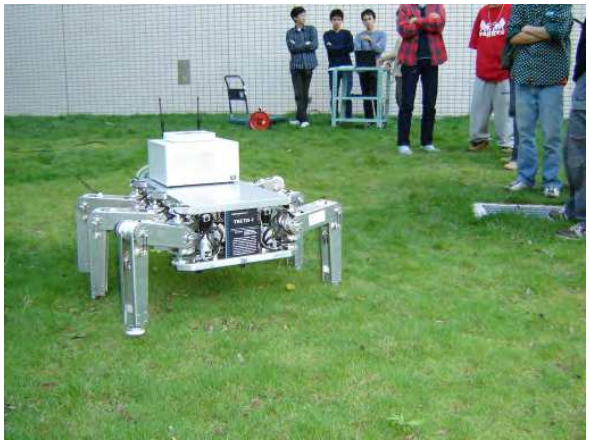

Fig. 1. The developed six-legged walking robot

Figure 1 shows our six-legged walking robot. The driving mechanism for each leg is a hybrid type mechanism composing a DC motor and a harmonic slowdown device through a rubber belt. Some accessories, such as computers, sensors, motor drive drivers and one AC power supply are mounted on the body of robot.

Figure 2 shows the schematic diagram of the robot with the detail measurements of its body. As shown, this robot is designed with three joints in each leg. By controlling the output torque of the motor for driving these three joints, the walking gait can be designed freely. θ_1~ θ_3 in Fig.1 show the rotation angles of the three joints, and each of them has a range of -90deg~ 270deg. This flexibility in foot is advantage for robot to walk on the irregular terrain. Each parameter encompassing the weight of each part of robot and the selected rated torque of the motor are shown in Table 1.

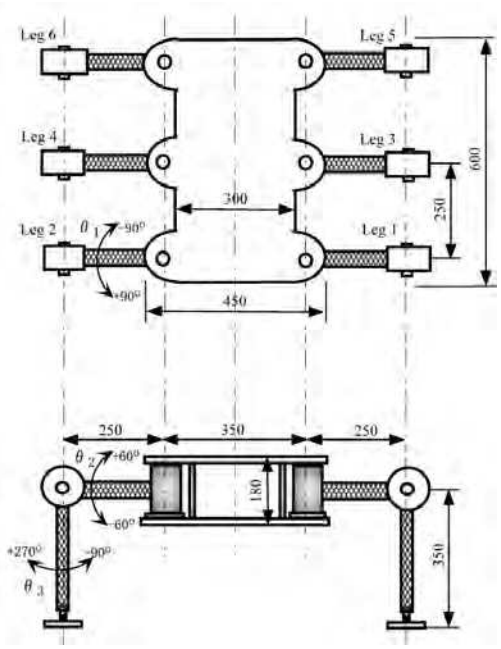

Fig. 2. Schematic diagram of the robot

Total weight [kg]	51.0
Loadable weight [kg]	40.0
Reduction ratio of harmonic drive β_1	80
Reduction ratio of harmonic drive β_2	120
Reduction ratio of harmonic drive β_3	80
Reduction ratio of timing belt γ_1	2.0
Reduction ratio of timing belt γ_1	4.0
Reduction ratio of timing belt γ_1	4.2
Rated torque of DC motor τ_{r1} [Nm]	0.14
Rated torque of DC motor τ_{r2} [Nm]	0.20
Rated torque of DC motor τ_{r3} [Nm]	0.14

Table 1. Specifications of the Robot

3. Virtual Compliance Control

3.1 Basic Controlling Expression

In this section, we introduce the conventional compliance control for the target trajectory tracking of the foot tip. The motion equation for the robot's legs with three joints can be expressed as follows.

$$\mathbf{M}(\theta)\ddot{\theta} + \mathbf{C}(\theta,\dot{\theta}) + \mathbf{D}\dot{\theta} + \mathbf{K}\theta + \mathbf{P}(\theta) = \boldsymbol{\tau} + \mathbf{J}^T(\theta)\mathbf{F} \tag{1}$$

where, θ=[θ_1 θ_2 θ_3]^T is a vector of three joints of a leg, $\mathbf{M}(\theta)$ is the inertia matrix, $\mathbf{C}(\theta,\dot{\theta})$ is the item considering centrifugal force and coriolis force, **D** is the coefficient matrix of viscous friction, **K** is the coefficient matrix of stiffness friction, **P** is the item of gravity, $\boldsymbol{\tau}$ is the driving torque of the motor, $\mathbf{J}^T$ is the jacobian matrix, and **F** is the item representing the external force added to the foot tip.

According to Eq.(1), the driving input torque to the motors can be written as

$$\boldsymbol{\tau} = \mathbf{M}(\theta)\ddot{\theta} + \mathbf{h}(\theta,\dot{\theta}) - \mathbf{J}^T(\theta)\mathbf{F} \tag{2}$$

$$\mathbf{h}(\theta,\dot{\theta}) = \mathbf{C}(\theta,\dot{\theta}) + \mathbf{D}\dot{\theta} + \mathbf{K}\theta + \mathbf{P}(\theta)$$

Where, we define $\mathbf{p}_e$ as a error vector between the target trajectories and the real trajectories based on the foot's coordinates.

$$\mathbf{p}_e = \begin{bmatrix} X - X_r \\ Y - Y_r \\ Z - Z_r \end{bmatrix} \tag{3}$$

$\mathbf{p}_e$ obtained from above expression is used for compliance function between the force acting on foot. It is possible to control the foot trajectory tracking.

$$\mathbf{F} = \mathbf{C}_c\dot{\mathbf{p}}_e + \mathbf{K}_c\mathbf{p}_e \tag{4}$$

substituting Equations(3) and (4) into Eq. (2), we can obtain the control input torque as follows:

$$\boldsymbol{\tau} = \mathbf{M}(\theta)\ddot{\theta} + \mathbf{h}(\theta,\dot{\theta}) - \mathbf{J}^T(\theta)\left(\mathbf{C}_c\dot{\mathbf{p}}_e + \mathbf{K}_c\mathbf{p}_e\right) \tag{5}$$

This expression is a basic control equation for the conventional compliance control.

3.2 Virtual Compliance Force

In this chapter, we introduce to add a virtual compliance force to change the trajectory of the foot before the foot contacts the ground. The advantage of adding the virtual compliance force is that the relative velocity between the foot and the ground when landing ground becomes zero, and then the contact collision can be decreased.

Moreover, this virtual compliance is effective when leg takes off the ground. The conventional compliance control have a problem that the load of bottom of foot rapidly become zero when the foot taking off the ground, and the unbalance of the body happen rapidly too. So it need that our proposed virtual force can prevent unbalance to reduce foot load slowly. Where, we install a proximity sensor on the back side of the foot, and its effective range is set as 3 cm. Fig. 3 shows the outline model of the robot leg include proximity sensor and virtual force. Here, the proposed virtual compliance force is calculated using the **q** that is vector from root of leg to foot.

$$\mathbf{F}_v = \mathbf{C}_v\dot{\mathbf{q}} + \mathbf{K}_v\mathbf{q} \tag{7}$$

Where, $\mathbf{F}_v$ is a virtual compliance force matrix, $\mathbf{C}_v$ is a virtual viscosity gain matrix, $\mathbf{K}_v$ is a virtual stiffness gain matrix, Eq. (6) can work effectively if the foot orbit far from the ideal one, so it is able to decelerate rapidly when proximity sensor perceives the obstacle. Fig. 4 and Fig. 5 are showing a frame format of proximity sensor changing.

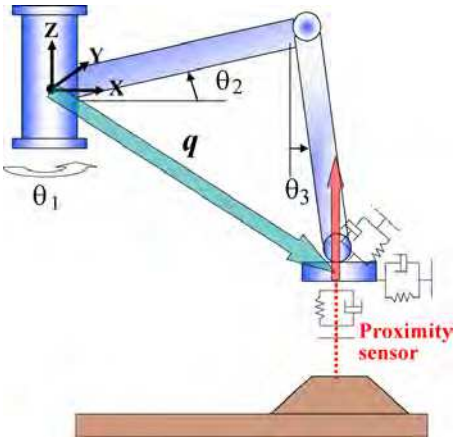

Fig. 3. Virtual compliance force

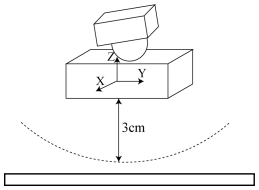

Fig. 4. Sensor off

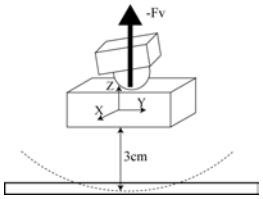

Fig. 5. Sensor on

However, this virtual force is needed while foot is near the objects and sensor is on, if the foot moves far away from the ground and obstacle, this virtual force is not only unnecessary but also disturbs a smooth track along the ideal orbit. So that, we rewrite $\mathbf{F}_v$ as follow.

$$\mathbf{F}_v = \begin{cases} 0 & (\text{sensor off}) \\ \mathbf{C}_v\dot{\mathbf{q}} + \mathbf{K}_v\mathbf{q} & (\text{sensor on}) \end{cases} \tag{6}$$

This virtual force divided in two cases to do flexible correspondence at the situation change. Concretely, when the sensor is off the virtual force $\mathbf{F}_v$ is zero, and when the sensor is on the virtual force $\mathbf{F}_v$ starts. Submitting the $\mathbf{F}_v$ into Eq. (5), we can get the control torques for the three joints of one leg of multi-legged robot as follows.

$$\boldsymbol{\tau} = \mathbf{M}(\theta)\ddot{\theta} + \mathbf{h}(\theta,\dot{\theta}) - \mathbf{J}^T(\theta)\left(\mathbf{C}_c\dot{\mathbf{p}}_e + \mathbf{K}_c\mathbf{p}_e - \mathbf{F}_v\right)$$
$$\boldsymbol{\tau} = \mathbf{M}(\theta)\ddot{\theta} + \mathbf{h}(\theta,\dot{\theta}) - \mathbf{J}^T(\theta)\left(\mathbf{C}_c\dot{\mathbf{p}}_e + \mathbf{K}_c\mathbf{p}_e - \mathbf{C}_v\dot{\mathbf{q}} - \mathbf{K}_v\mathbf{q}\right) \tag{8}$$

4. Phased Compliance Control

In the conventional compliance control, because the compliance gain matrix keep constant in all phases of the movement of the swing leg, it is impossible to response all unexpected situation walking on irregular terrain where needed stability and flexible correspondence. Therefore, in this paper, we divide the walking movement into six phases shown as in Fig. 6, the compliance gain matrix $\mathbf{C}_v$, $\mathbf{K}_v$, $\mathbf{C}_c$, $\mathbf{K}_c$ are variable in different phase.

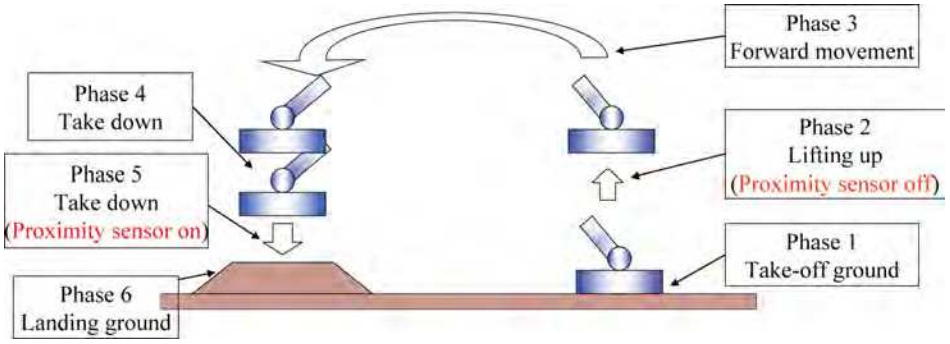

Fig. 8. Divided walking motion into six phases

Phase 1 is a period from the foot starts taking off ground until the proximity sensor becomes off. In this phase, the main purpose is to slowly decrease the force load of the foot using the virtual compliance force. By adjusting virtual compliance gain matrix $\mathbf{C}_v$, $\mathbf{K}_v$ the virtual force is generated to press the leg against ground and a smooth decrease in force load of the foot is achieved by slowly decreasing that virtual force. As a result, the generation of the impact power and a sudden balance-off of robot's body can be suppressed.
Phase 2 is a leg lifting phase that the control from the proximity sensor becomes off until end position of lifting leg. This phase is important to follow the ideal orbit to recover the phase 1's delay quickly. So the normal compliance gain $\mathbf{C}_c$, $\mathbf{K}_c$ are enlarged, and the virtual compliance gain $\mathbf{C}_v$, $\mathbf{K}_v$ make decrease to 0 by the time when the proximity sensor becomes off.
Phase 3 and 4 are the horizontal and descent movement of leg until the proximity sensor becomes on. These two phases are important to follow the ideal orbit, but horizontal movement have a danger of colliding with the obstacle toward x and y axially. As the measures, if the external force $\mathbf{F}$ is added to the foot, the normal compliance gain $\mathbf{C}_c$, $\mathbf{K}_c$ in the x and y directions becomes small to avoid the obstacle.
Phase 5 is a foot descend period from proximity sensor becomes on until the foot contacts with ground or obstacle. In this phase, deceleration of foot is put in preparation for contact with the object, and it has aimed to weaken the impact force when colliding. So that, the virtual compliance gain matrix $\mathbf{C}_v$, $\mathbf{K}_v$ are greatly taken and the sudden deceleration is enable.
Phase 6 is a control phase for the support leg that is not necessary to use virtual compliance. The normal compliance gain $\mathbf{C}_c$, $\mathbf{K}_c$ are set large because it is necessary not only to follow the orbit of the support leg but also to support the weight of the body. In this paper, to this phase 6, we use a posture and vibration control based on virtual suspension model

introduced in section 5 to generate torques for support legs to realize the stable posture of robot.
Smooth movement suitable for the situation is possible to use phased division of such phased compliance control.

5. A Hierarchical Control System Combined the Phased Compliance Control with a Posture and Vibration Control

However, because the phased compliance control is applicable only to swing legs of multi-legged walking robot, we designed a hierarchical control system for multi-legged walking robot, which is combined the proposed phased compliance control with a posture and vibration control based on virtual suspension model, to realize the stable walking on unknown rough terrain.
The control block diagram of the hierarchical control system is shown as in Fig. 9. According of this control block diagram, there are two parts in control system. The first part is a position control for swing legs using the phased compliance control designed in sections 3 and 4. The second part is posture and vibration control of robot body for support legs. In this part, the VSM and SMC are virtual suspension model and sliding mode control for constraining the robot's posture and damping the changes of its posture (Q. Huang, et al., 2004). And the CSM is Coordinate Shift Method proposed by our study, which can calculate the forces of each support leg to equilibrate the posture changes. The calculated forces are multiplied with the jacobian matrix, and are transported to the each joints of support leg. Where, we introduce the second part as follows.

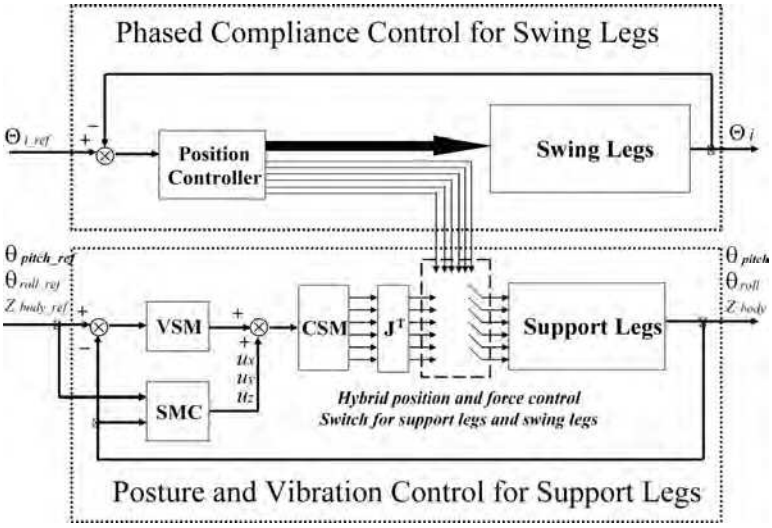

Fig. 9. A hierarchical control system combined phased compliance control with posture and vibration control

5.1 Suspension Control Using Sliding Mode Control Based on the Virtual Dynamic Model

To restrain the vibration of robot body, a suspension model is built in this study. As shown in Fig. 10, the ground is assumed to be rigid; a suspension model of one degree of freedom with virtual springs and dampers is designed in the vertical direction, the direction of the pitch angle, and the direction of the roll angle, respectively (Q. Huang, et al., 2004). In Fig. 10, the vertical direction of the robot body is defined to be the z coordinate axis, the advancing direction of the robot is defined to be the y coordinate axis, and the direction crosshatched to the above two directions is defined to be the x coordinate axis.

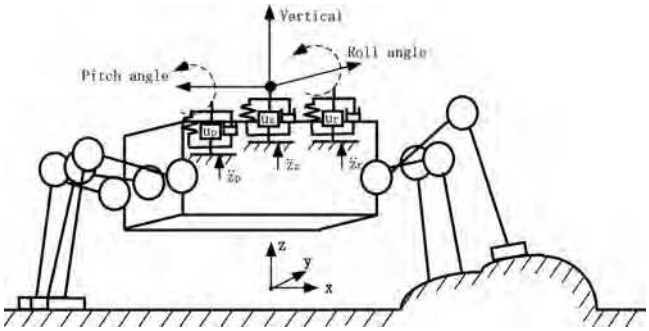

Fig. 10. The virtual suspension model considering of active control input and disturbances

Here, z, θ_p, θ_r are defined to be the changes in the vertical direction, the directions of the pitch angle and the roll angle from the balance place, respectively. In order to improve the excessive characteristic of the system response and to minify the overshot, the damping coefficient ζ is selected to be within 0.7~1.0. Besides, the natural angular frequency ω_n is enlarged as much as possible to avoid resonance because the vibrations in the vertical direction, the directions of the pitch angle and the roll angle, the disturbances from collisions and slippage between the ground and the robot leg, and dynamic changes of the supported weight and the centre of gravity are within low frequency. Furthermore, because of the enlarging of the natural angular frequency ω_n, good stability and excessive response characteristics within a wide frequency band can be realized in the virtual suspension dynamic system. Therefore, in this study, the natural angular frequency ω_n and the damping coefficient ζ are selected respectively as follows,

$$\omega_{nx} = 250 \qquad \omega_{ny} = 250 \qquad \omega_{nz} = 60$$
$$\varsigma_x = 0.800 \qquad \varsigma_x = 0.800 \qquad \varsigma_x = 0.800 \tag{8}$$

The body weight and rotary moment of inertia of the six-legged walking robot in this study are

$$I_x = 1.072[\mathrm{kgm}^2] \qquad I_y = 0.906[\mathrm{kgm}^2] \qquad \mathrm{M} = 16.753[\mathrm{kg}]$$

According of the natural angular frequency ω_n and the damping coefficient ζ, the parameters of the proposed virtual dynamic model are as follows,

$$K_z = 167530.0[N/m] \qquad C_z = 2680.5[Ns/m]$$
$$K_p = 67000.0[Nm/rad] \qquad C_p = 428.8[Nms/rad]$$
$$K_r = 56643.8[Nm/rad] \qquad C_r = 428.8[Nms/rad]$$

Where, the control input u_x, u_y, and u_z were designed by using sliding mode control (Q. Huang, et al., 2004; Q. Huang, et al., 2007; K. Nonami and H. Tian, 1994; X. Zhong, et al., 2007). So that, the motion equations for the vertical direction, the directions of the pitch angle of robot body and the roll angle of robot body are defined as

$$\left(M + \Delta M(t,\theta_{sw})\right)\ddot{z} = -K_z z - C_z \dot{z} + u_z + \ddot{z}_z \tag{9}$$

$$\left(I_x + \Delta I_x(t,\theta_{sw})\right)\ddot{\theta}_p = -K_p \theta_p - C_p \dot{\theta}_p + u_p + \ddot{z}_p \tag{10}$$

$$\left(I_y + \Delta I_y(t,\theta_{sw})\right)\ddot{\theta}_r = -K_r \theta_r - C_r \dot{\theta}_r + u_r + \ddot{z}_r \tag{11}$$

In this study, we designed the same control system for the vertical direction, the direction of the pitch angle, and the direction of the roll angle. Here, only the designed sliding mode control of one-type style servo system in the direction of the pitch angle is introduced. In the designed sliding mode control, the integral value of the difference between the target pitch angle and the actual pitch angle is defined to be a new state variable. Substituting the new state variable z_{en} into Eq. (9), an extended state equation can be derived. The extended state equation and the switching function σ are

$$\begin{cases} \dot{\boldsymbol{x}}_e = A\boldsymbol{x}_e + \boldsymbol{B}\boldsymbol{u} + \boldsymbol{Q}r + \boldsymbol{F}d \\ z_{en} = \int (r - \theta_p)dt \\ \boldsymbol{s} = \boldsymbol{S}\boldsymbol{x}_{en} \end{cases} \tag{12}$$

$$\boldsymbol{x}_e = [z_{en} \quad \theta_p \quad \dot{\theta}_p]^T \qquad d = \ddot{z}_p$$

and, A, B, Q are expressed by

$$\boldsymbol{A} = \begin{bmatrix} 0 & -1 & 0 \\ 0 & 0 & 1 \\ 0 & -K_p / I_p & C_p / I_p \end{bmatrix} \quad \boldsymbol{B} = \begin{bmatrix} 0 \\ 0 \\ 1/I_p \end{bmatrix} \quad \boldsymbol{Q} = \begin{bmatrix} 1 \\ 0 \\ 0 \end{bmatrix}$$

Where, r is the target value of the pitch angle, and is zero here. d is the term denoting the disturbances. In sliding mode control, if the equivalent control input u_{eq} is without consideration of disturbances, from $\sigma = \dot{\sigma} = 0$, the linear input u_{lp} can be obtained from

$$u_{lp} = u_{eq} = -(\boldsymbol{SB})^{-1}(\boldsymbol{SA}\boldsymbol{x}_e + \boldsymbol{SQ}r) \tag{13}$$

Switching matrix S is solved by using the solution of the Riccati equation. The real component of the eigenvalue of the equivalent control system is -50 here. The nonlinear input of the sliding mode control u_{nlp} is expressed by

$$u_{nlp} = -k(\boldsymbol{SB})^{-1}\frac{\sigma}{|\sigma| + \eta} \tag{14}$$

Nonlinear input u_{nlp} compensates for the uncertainty of the system, as the control input to constrain the system state variables within the switching plane. Here, the coefficient to repress the disturbances k = 8600, and the coefficient to avoid the chattering η = 0.1. Therefore, the input of the sliding mode control is u, which is composed of the linear control input u_{lp} and the nonlinear control input u_{nlp}.

6. Experiment and Discussion

6.1 Preparations for the Experiment

Because the purpose of this study is to restrain the vibration in the z direction and the directions of the pitch angle and the roll angle of the robot body when the robot walks, it is necessary to obtain the outputs in these three directions. As to the output angles in the directions of the pitch angle and the roll angle, they were measured by a slant sensor. In the vertical direction, the output can be calculated from the size of the robot body and the forces in the vertical direction of each leg. Here, in order to save the cost, we don't use the force sensor to observe the forces of each leg, rather than use the motor pseudo-torque.

6.1.1 The Observation by Using the Motor Pseudo-Torque

The motor torque is obtained by multiplying a torque coefficient to the motor electric current. However, because the vibration caused by noise is too big, instead of the motor torque, a pseudo-torque is used as the input torque. The pseudo-torque is the calculated torque of one sampling time before. In the servo electric circuit, the calculated pseudo-torque approximates to the actual consumed torque. Therefore, using the pseudo-torque, there is no the influence by the noise. Of course, a delay of one sampling time arises simultaneously. The influence caused by the delay can be ignored if the sampling time is small enough.

6.1.2 Conversion from Motor Torque to Force of the Tip of Each Leg

The force of the tip of leg, $\boldsymbol{f} = [f_x \quad f_y \quad f_z]^T$, was calculated from the size of each link and the inverse of Jacobi matrix. The force of the tip of leg can be obtained as expressed as follows.

$$\boldsymbol{f} = \left(\boldsymbol{J}^T\right)^{-1} \boldsymbol{\tau} \tag{15}$$

$$f_{asis} = \tau_2 + \frac{l_2 \sin\theta_2 + l_3 \cos(\theta_2 + \theta_3)\tau_3}{l_3 \cos(\theta_2 + \theta_3)} \tag{16}$$

$$f_z = \frac{1}{l_2 \tan(\theta_2 + \theta_3) \sin\theta_2 + \cos\theta_2} f_{asis} \tag{17}$$

$$f_y = \frac{1}{\tan\theta_1}\left(\frac{\tau_1}{l_2 \cos\theta_2 + l_3 \sin(\theta_2 + \theta_3)}\right) + \frac{\tau_2}{l_3 \cos(\theta_2 + \theta_3)} - \tan(\theta_2 + \theta_3) f_z \tag{18}$$

$$f_x = -\frac{\tau_1}{\sin\theta_1}\left(\frac{1}{l_2 \cos\theta_2 + l_3 \sin(\theta_2 + \theta_3)}\right) + \frac{1}{\tan\theta_1} f_y \tag{19}$$

6.2 Experimental Results

The experiments were performed by two kinds of gaits. The first is with one swing leg and five support legs called as pentapod gait; the second is with three swing legs and three support legs called as tripod gait. According of the walking experiments, the stable walking of the pentapod gait and the tripod gait were realized shown as in Fig. 11 and Fig. 12. Where, the experimental results of these two kinds of gait are introduced and discussed as follows.

Fig. 11. Pentapod gaite walking

Fig. 12. Tripod gait walking

6.2.1 Pentapod gait

Pentapod gait is excellent in stability instead of slow the speed because always five legs are the support legs. Details of walking operation are shown Fig. 13. According to figure the legs are sequentially moved. Each parameter in pentapod gait shows as follows.

Length f tride = 180 [mm]
Max height of foot = 80 [mm]
Time of one step = 0.75 [s]

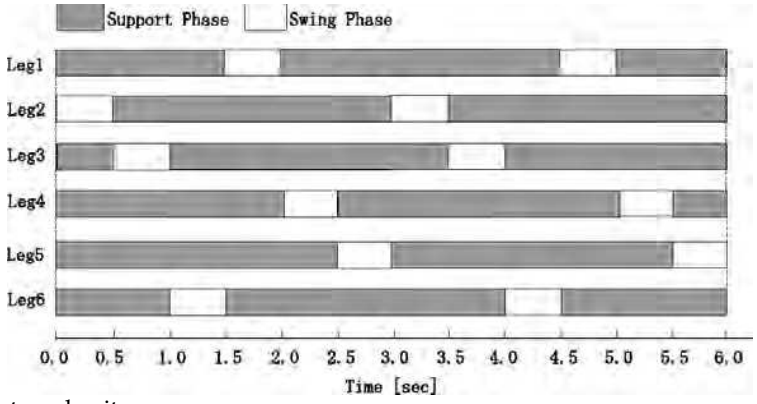

Fig. 13. Pentapod gait

The results of walking with pentapod gait are shown in Fig. 14~Fig. 19. In these figures, the dotted lines show the results of the conventional compliance control using the Eq. (5); the solid lines show the results of our proposed phased compliance control with virtual force.

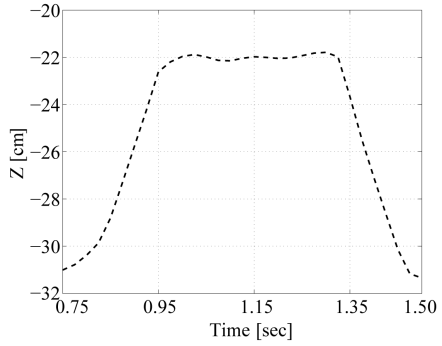

Fig. 14. Foot position change in Z direction using the conventional position control

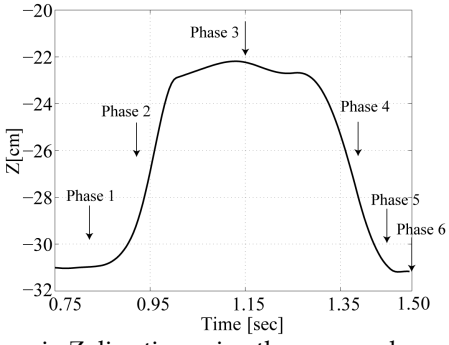

Fig. 15. Foot position change in Z direction using the proposed compliance control

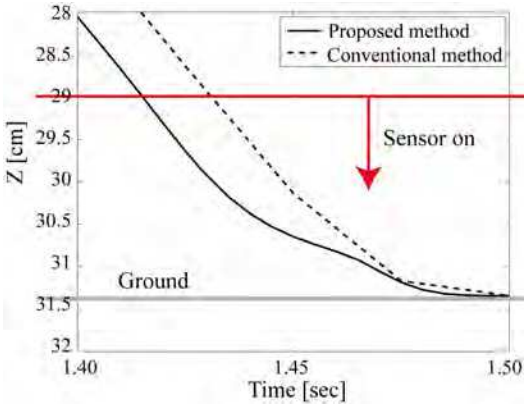

Fig. 16. Close-up of the landing ground in Z direction

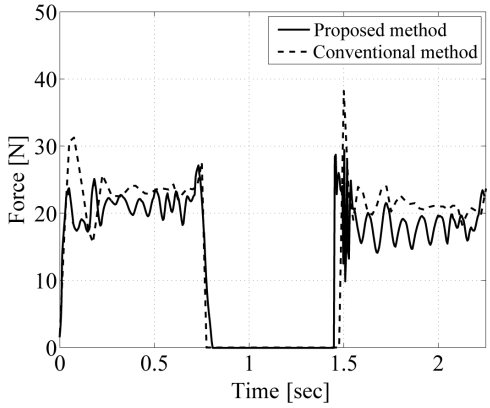

Fig. 17. Force load of the foot of leg 3

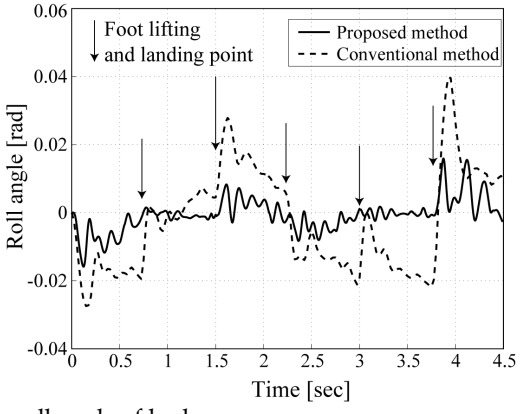

Fig. 18. Changes of the roll angle of body

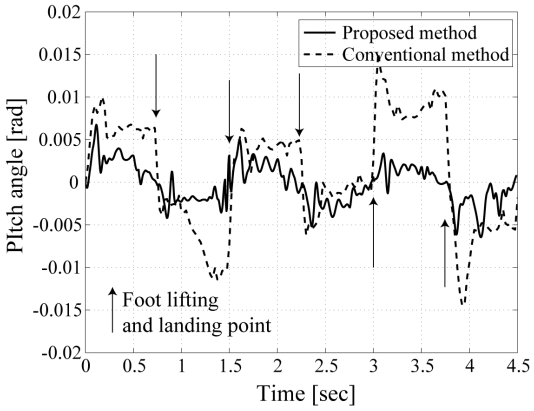

Fig. 19. Changes of the pitch angle of body

Firstly, according of Figures 14 and 15, about the changes in Z direction of the end position of the swing foot, both the proposed phased compliance control with virtual and the conventional compliance control are almost realized the ideal position finally. But in the time 0.75 sec~0.95 sec of lifting leg and 1.30 sec~1.50 sec of landing leg, the delay in the proposed phased compliance control with virtual force occurred that caused foot load slowly decreasing at phase 1 and slowing increasing at the phase 5 and phase 6 shown as in Fig. 17, so the changes of pitch angle and roll angle of the robot body become smaller than the results of the conventional compliance control shown as in Fig. 18 and Fig. 19.
The close-up of Z direction coordinates in the time 1.3 sec~1.5 sec of landing swing leg is shown Fig. 16. We can see that the proposed compliance control with virtual force generates a virtual force in the positive direction of Z direction coordinates at the time as the proximity sensor switched on.
And then, in Fig. 17, we can see the impact force between the foot and the terrain is reduced about 70% using our proposed method than the one using the conventional compliance control. And, according of Fig. 18 and Fig. 19, in the case of the proposed phased compliance control with virtual force, the changes of pitch angle and roll angle of the robot body are decreased about 50% than the results of the conventional compliance control. Especially, the biggest changes of pitch angle and roll angle of the robot body at the switch timing of lifting and landing the leg, have been decreased, because the control in phase 1, phase 5 and phase 6 work well using the virtual compliance force and impact force is decreased.

6.2.2 Tripod gait

Details of walking operation of tripod gait are shown Fig. 20. Each parameter in tripod gait shows as follows.

Length of stride = 180 [mm]
Max height of foot = 80 [mm]
Time of one step = 0.75 [s]

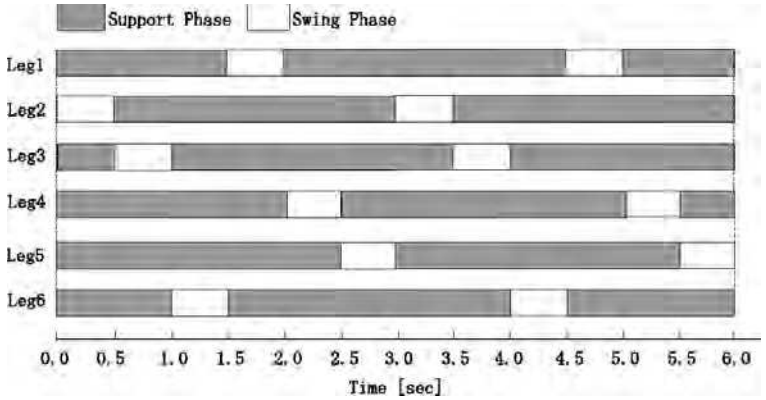

Fig. 20. Tripod gait

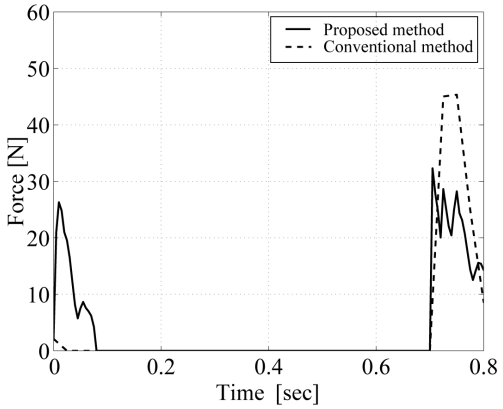

Fig. 21. Force load of the foot of leg 1

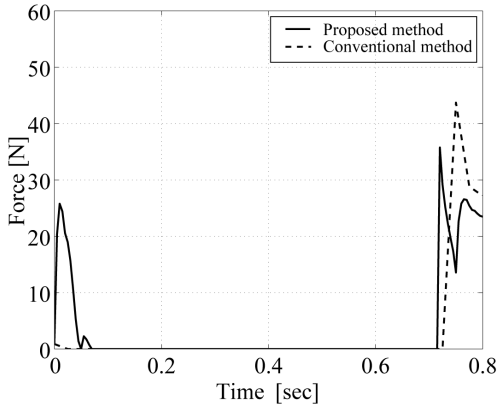

Fig. 22. Force load of the foot of leg 4

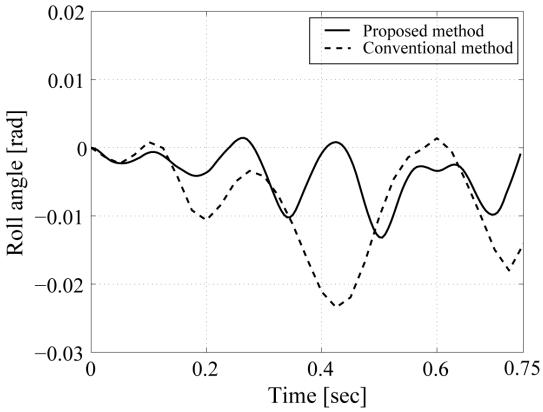

Fig. 23. Changes of the roll angle of body

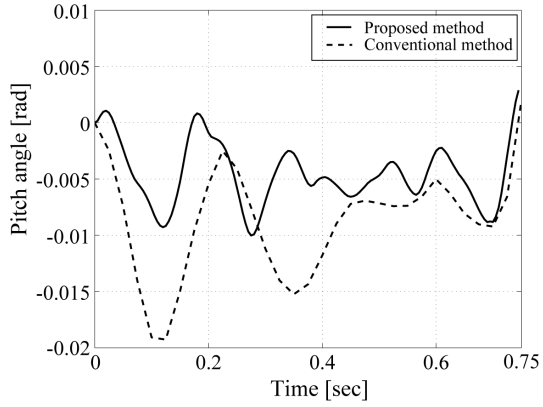

Fig. 24. Changes of the pitch angle of body

As the same results of the pentapod gait, in the time 0.0 sec~0.1 sec of lifting leg and 0.70 sec~0.78 sec of landing leg, the delay in the proposed phased compliance control with virtual force occurred that caused foot load slowly decreasing at phase 1 and slowing increasing at the phase 5 and phase 6 shown as in Fig. 21 and Fig. 22, so the changes of pitch angle and roll angle of the robot body become smaller than the results of the conventional compliance control shown as in Fig. 23 and Fig. 24. The impact force between the foot and the terrain is reduced about 70%, the changes of pitch angle and roll angle of the robot body are decreased about 50% using our proposed method comparing with the results using the conventional compliance control.

According of the above walking experimental results of pentapod gait and tripod gait, we can see the efficiency of our proposed compliance control with virtual force in aspect of decreasing the impact force between the foot and the terrain for multi-legged robot.

7. Conclusion

For the multi-legged walking robot, in order to decrease impact force between the foot and the terrain when the foot lifting and landing to realize its better stability, we did the following studies.

We introduced a phased compliance control using virtual compliance force for multi-legged walking robot, which can effectively reduce the impact force when the robot walks. Concretely, we add a virtual compliance force to change the trajectory of the foot before the foot contacts the ground based on the conventional compliance control. And then, we divide the walking movement into six phases to adjust the compliance gain to realize reducing the impact force when robot lifting and landing leg in the same walking speed as the conventional compliance control.

We designed a hierarchical control system for multi-legged walking robot, which is combined the proposed phased compliance control with a posture and vibration control based on virtual suspension model, to realize the stable walking on unknown rough terrain.

According of the walking experimental results of pentapod gait and tripod gait using a six-legged robot, the impact force between the foot and the terrain is reduced about 70%, the changes of pitch angle and roll angle of the robot body are decreased about 50% using our introduced method comparing with the results using the conventional compliance control, so the effectiveness of the proposed method for multi-legged walking robot was verified.

8. References

D. Wettergreen, C. Thorpe (1996). Developing Planning and Active Control for a Hexapod Robot, *Proc. 1996 IEEE Int. Conf. on Robotics and Automation*, pp. 2718-2723.

T. Kubota, H. Katoh, I. Nakatani (2000). Walking Rover with Multiple Legs for Planetary Exploration, *Proc. of the Third Int. Conf. on Climbing and Walking Robots*, pp. 795-788.

Q. Huang, K. Nonami, etc. (2000). CAD Model Based Autonomous Locomotion of Quadruped Robot by Using Correction of Trajectory Planning with RNN, Special Issue on Frontiers of Motion and Vibration Control, *JSME International Journal*, Series C, Vol. 43, No. 3, pp. 653-663.

Q. Huang, K. Nonami (2002). Neuro-Based Position and Force Hybrid Control of Six-Legged Walking Robot, Special Issue on Modern Trends on Mobile Robotics, *Journal of Robotics and Mechatronics*, Vol. 14, No. 4, pp. 534-543.

Q. Huang, K. Nonami (2003). Humanitarian Mine Detecting Six-Legged Walking Robot and Hybrid Neuro Walking Control with Position/Force Control, Special Issue on Computational Intelligence in Mechatronic Systems, *Mechatronics*, Elsevier, Vol. 13, No. 8-9, pp. 773-790.

K. Nonami, Q. Huang, etc. (2003). Development and Control of Mine Detection Robot COMET-II and COMET-III, *JSME International Journal*, Series C, Vol. 46, No. 3, pp. 881-890.

Q. Huang, M. Yanai, K. Oon, K. Nonami (2004). Robust Control of Posture and Vibration Based on Virtual Suspension Model for Six-Legged Walking Robot, *Proceedings of the 7th international conference of Motion and Vibration Control*, Washington University in St. Louis, America, CD-ROM, No. 41.

Q. Huang, Y. Fukuhara, X. Chen (2007). Posture and Vibration Control Based on Virtual Suspension Model Using Sliding Mode Control for Six-Legged Walking Robot, Special Issue on New Trends of Motion and Vibration Control, *Journal of System Design and Dynamics*, the JSME Dynamics, Mesurement and Control Division, Vol. 1, No. 2, pp. 180-191.

J. Huang, I. Toda, M. Matsuura (2002). Control a Redundant Robot Using Visual Information: Avoidance Control of a Moving Obstacle, *Transactions of the Japan Society of Mechanical Engineers*, Series C, Vol. 68, No. 674, pp. 2999-3006.

R. Quint (1998). Active leg compliance for passive walking, *Proceedings of the 1998 IEEE International Conference on Robotics and Automation*.

V. Mut, O. Nasisi, R. Carelli, B. Kuchen (1998). Tracking Adaptive Impedance Robot Control With Visual Feedback, *Proceedings of the 1998 IEEE International Conference on Robotics and Automation*.

X. Chen, H. Kano (2005). Dynamic Vision Based Motion Recovery, *International Journal of Innovative Computing, Information and Control*, Vol. 1, No. 3, pp. 509-525.

T. Tsuji, H. Akamatsu, M. Kaneko (1997). Non-Contact Impedance Control for Redundant Manipulators Using Visual Information, *Proceedings of the 1997 IEEE International Conference on Robotics and Automation*.

Q. Huang, K. Oka, X. Chen (2008). Phased Compliance Control with Virtual Force for Six-legged Walking Robot, Special Issue on New Trends in Advanced Control and Applications, *International Journal of Innovative Computing, Information and Control*, Vol. 4, No. 12, pp. 3359-3373.

K. Nonami, H. Tian (1994). Sliding Mode Control, CORONA Publishing Co., Ltd. (In Japanese)

X. Zhong, H. Xing and K. Fujimoto (2007). Sliding Mode Variable Structure Control for Uncertain Stochastic Systems, *International Journal of Innovative Computing, Information and Control*, Vol. 3, No. 2, pp. 397-406.

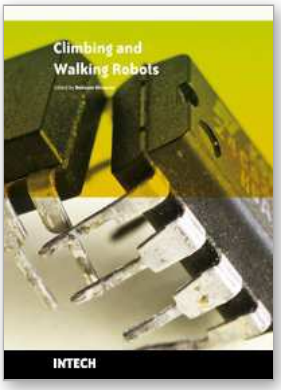

Climbing and Walking Robots

Edited by Behnam Miripour

ISBN 978-953-307-030-8
Hard cover, 508 pages
Publisher InTech
Published online 01, March, 2010
Published in print edition March, 2010

Nowadays robotics is one of the most dynamic fields of scientific researches. The shift of robotics researches from manufacturing to services applications is clear. During the last decades interest in studying climbing and walking robots has been increased. This increasing interest has been in many areas that most important ones of them are: mechanics, electronics, medical engineering, cybernetics, controls, and computers. Today's climbing and walking robots are a combination of manipulative, perceptive, communicative, and cognitive abilities and they are capable of performing many tasks in industrial and non- industrial environments. Surveillance, planetary exploration, emergence rescue operations, reconnaissance, petrochemical applications, construction, entertainment, personal services, intervention in severe environments, transportation, medical and etc are some applications from a very diverse application fields of climbing and walking robots. By great progress in this area of robotics it is anticipated that next generation climbing and walking robots will enhance lives and will change the way the human works, thinks and makes decisions. This book presents the state of the art achievments, recent developments, applications and future challenges of climbing and walking robots. These are presented in 24 chapters by authors throughtot the world The book serves as a reference especially for the researchers who are interested in mobile robots. It also is useful for industrial engineers and graduate students in advanced study.

How to reference

In order to correctly reference this scholarly work, feel free to copy and paste the following:

Qingjiu Huang (2010). Softly Stable Walk Using Phased Compliance Control with Virtual Force for Multi-Legged Walking Robot, Climbing and Walking Robots, Behnam Miripour (Ed.), ISBN: 978-953-307-030-8, InTech, Available from: http://www.intechopen.com/books/climbing-and-walking-robots/softly-stable-walk-using-phased-compliance-control-with-virtual-force-for-multi-legged-walking-robot

INTECH
open science | open minds

InTech Europe
University Campus STeP Ri
Slavka Krautzeka 83/A
51000 Rijeka, Croatia
Phone: +385 (51) 770 447
Fax: +385 (51) 686 166

InTech China
Unit 405, Office Block, Hotel Equatorial Shanghai
No.65, Yan An Road (West), Shanghai, 200040, China
中国上海市延安西路65号上海国际贵都大饭店办公楼405单元
Phone: +86-21-62489820
Fax: +86-21-62489821